Numerical simulation of different combustion regimes in a laboratory combustor

Paweł Rodak
pawel.rodak@vp.pl

Instituto Superior Técnico, Universidade de Lisboa, Portugal

January 2017

The present dissertation reports the numerical simulations of a small-scale natural gas combustor operating in the flameless oxidation (FLOX) combustion regime, where the oxidation of the fuel occurs in an atmosphere with relatively low oxygen concentration. Depending on the different configurations of the burner geometry, different combustion regimes may be observed. For this reason, the simulations have been performed for different burner configurations, to investigate their influence on the combustion process. All the calculations have been performed using the ANSYS Fluent v17.1 code. The combustion model applied for all the simulations was the Eddy Dissipation Concept (EDC) coupled with the detailed chemical mechanism DRM-19. The turbulence model was $k-\omega$ SST. The results of simulations are presented. For the configurations (A-E) corresponding to the experimental studies, numerical results have been compared to available measurement data. The numerical results show that the applied turbulence model is not able to accurately predict the decay of the air stream at the vicinity of the burner. The simulations of different burner configurations show that for smaller air inlet diameters, the reaction zone moves progressively closer to the burner and due to more intense mixing, the temperature field is more leveled. A similar conclusion can be made for the smallest tested distance between air and fuel nozzles L = 7.5 mm. The combustion could be characterized by the flameless oxidation regime for this distance, with lower maximum temperature and more uniform temperature field, whereas for the fuel inlet distance of 30 mm, high temperature regions, indicating the presence of a flame front, were identified.

Keywords: *FLOX combustion regime, Methane combustion, ANSYS Fluent, Numerical simulation, DRM-19, EDC*

INTRODUCTION

The technology of combustion has been developing for decades, but still there are a demand and room for further improvement and innovation. This concerns especially the methods for reduction of greenhouse gas (GHG) emissions, pollutant emissions such as nitrous oxides (NO_x), carbon oxide (CO), soot, unburned hydrocarbons (HC) and improving the efficiency of the combustion process.

In this field the improvements can be achieved with the help of flameless oxidation (FLOX) combustion regime. The use of natural gas as a fuel is increasing (IEA 2016). Natural gas is a fuel with several advantages over, for instance, coal. First of all, its combustion produces approximately 1.7 times less CO2 per 1 kWh. Natural gas is cleaner by itself, easy to transport and has high energy density. It can be combusted in gas-steam combined cycle (GSCC) reaching efficiencies of about 60 %, which is much higher than state of the art coal power plants.

Therefore the natural gas might become the fuel of the future, as the developed countries aim to reduce their emissions, improve the efficiency and become less dependent on coal.

FLOX combustion is a very promising technology, which could be applied for instance in land based gas turbines, boilers combustion chambers and domestic heating systems (Cavaliere and Joannon 2004). It is a regime characterized by a volumetric reaction zone, more uniformed temperature field and the absence of a thin flame front. The oxidation of fuel occurs in an atmosphere with relatively low oxygen concentration, which is the effect of strong flue gas recirculation ratio. As a result, this combustion regime results in low noise, negligible soot formation, reduced NOx and CO emissions in comparison with regular combustion (Veríssimo et al. 2011). The regime is often achieved with the use of preheated air, however, this is not mandatory requirement as shown by Kumar et al. (2002), Krishnamurthy et al. (2009), and Mi et al. (2009). Due to the low oxygen concentration, the reaction develops slower and over a larger region comparing to the traditional combustion process.

MATERIALS AND METHODS

Figure 2 shows a schematic of the combustor simulated in this study. The combustion chamber is a quartz glass cylinder with an inner diameter of 100 mm and a length of 340 mm. The quartz cylinder is insulated with a 30 mm thick ceramic fiber blanket. Only the numerical simulations have been performed for the purpose of this study, the experimental data are taken from the past studies of Veríssimo et al. (2011, 2013).

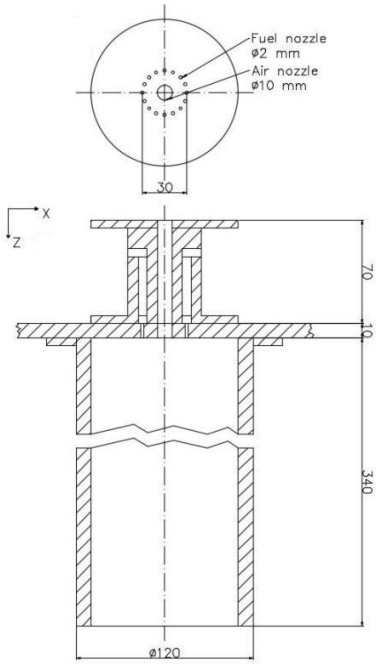

Fig. 1 Schematic of the combustor.

The burner is placed at the top end of the combustion chamber and the exhaust of the burned gasses is made by the bottom end. As seen in figure 1, the burner consists of a central orifice of 10 mm inner diameter, through which the combustion air is supplied, surrounded by 16 small orifices of 2 mm inner diameter each, positioned on a circle with a radius of 15 mm, for the fuel (methane) supply.

The combustion air is preheated by an electrical heating system that allows air inlet temperatures up to 700°C.

The central orifice has an adjustable inner diameter. In the study of Veríssimo et al. (2013), different settings were analyzed. Changing the air inlet diameter, while maintaining constant excess air coefficient λ, results in changes of the air inlet velocity. Predictions for these different settings have also been simulated and compared with available experimental data. The measurement points are presented in figure 2. For all the measurement points, the available data include mean temperature and species concentrations (NO_x, CO, CO_2, O_2).

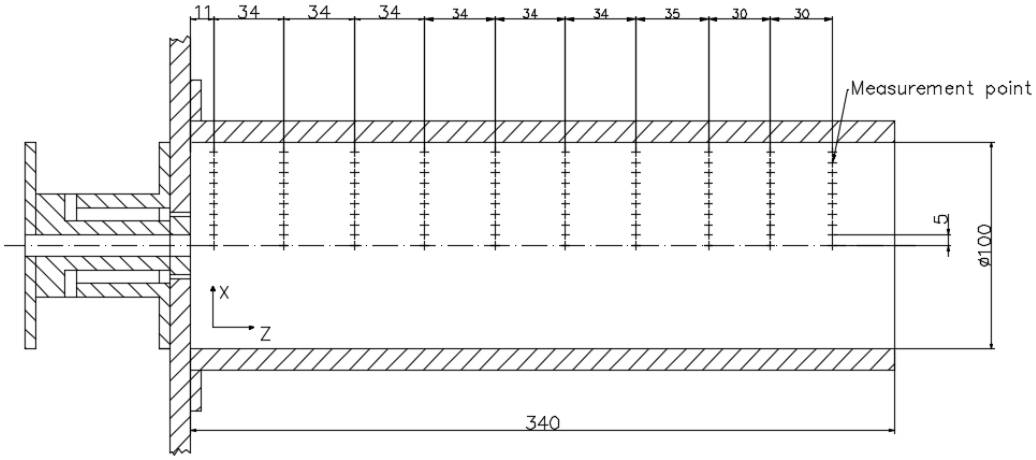

Fig. 2 Schematic of the combustor with the measurement points overlaid.

In order to monitor the main combustion zone inside the combustor, the chemiluminescence imaging was performed (Veríssimo et al. 2011). This technique aims to record the light emitted from the chemically excited OH, denoted OH*, which is an important intermediate species in the oxidation of hydrocarbon fuels. The OH radical is formed in the flame front, and this is why OH is a commonly used marker for this region.

MATHEMATICAL MODELING

The mathematical model is based on the numerical solution of the Favre-averaged governing equations for mass, momentum, and energy and on transport equations related to the turbulence and combustion models. Turbulence was modeled using the Shear Stress Transport (SST) $k-\omega$ model (Menter 1993), which involves the solution of transport equations for the turbulent kinetic energy and its specific dissipation rate, and combustion was simulated using the EDC (Magnussen, 1981) model. The EDC is able to use detailed finite-rate chemical kinetics in the simulation of turbulent reactive flows. Transport equations for the species are solved during the computational fluid dynamics (CFD) calculations.

A reaction mechanism DRM-19 (Kazakov and Frenklach) for the combustion of methane comprising 21 transported species and 84 chemical reactions was used.

The in-situ adaptive tabulation (ISAT) method (Pope, 1997) was used to reduce the computational cost of the chemical source term integration for the EDC method.

Thermal radiation was taken into account using the discrete ordinates method and the radiative properties of the participating medium were modeled using the weighted-sum-of-grey gases model, in which the spatial variation of the total emissivity is computed as a function of the H_2O and CO_2 local mass fractions and temperature.

COMPUTATIONAL DETAILS

The computational domain represents the interior of the combustor, in other words, the computational domain is a representation of volume filled in with the gas mixture. Due to the symmetrical design of the combustor and the symmetrical nature of the flow, the simulation can be performed for 1/16 (22,5^o) of the combustion chamber. The simulation of the whole combustion chamber would require far more computational time and would produce the same result, as can be achieved with the geometry representing 1/16 of the actual object. The inlet ducts were included in the geometry in order to develop the flow before the reactant gasses reach the combustion chamber. The mesh has approximately 40.000 cells. Further grid refinement did not yield significant changes in the results. As it can be seen in figure 3, the geometry was sliced into parts, which were meshed with different cell sizes. Such approach was implemented in order to provide finer meshing in the main region of the reaction zone, where higher gradients of temperature and velocity are expected. Apart from the central zone of the combustion chamber, the mesh was refined in the region near the side wall of the combustor chamber in order to improve the accuracy of the heat transfer simulation between the side wall of the combustor and the medium within the combustor. The mesh is presented in figure 3.

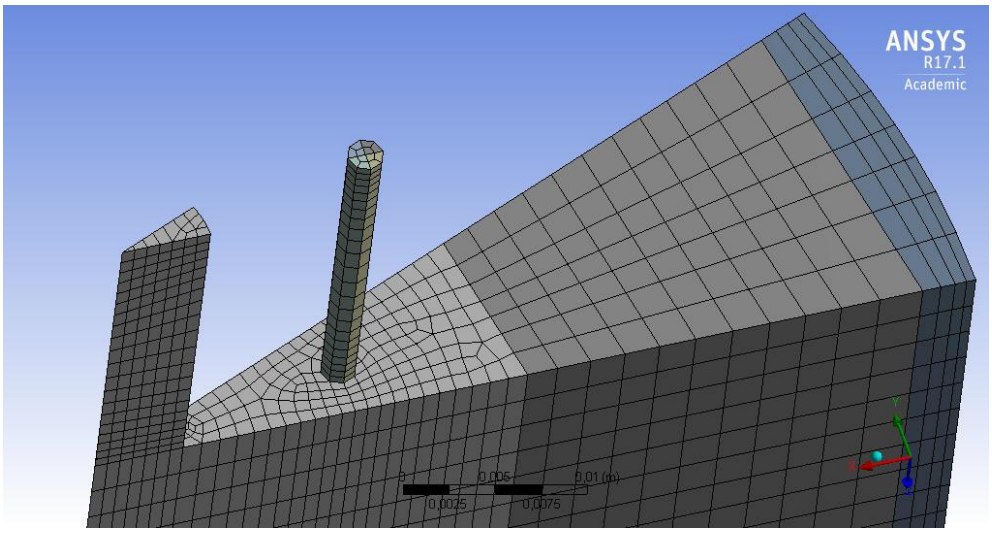

Fig. 3 Computational grid (air inlet diameter of 10 mm and the fuel inlet distance of 15 mm).

All of the governing equations were solved using a second-order upwind discretization scheme, and the SIMPLEC algorithm. The convergence criterion demanded that the sum of the residuals of the discretized equations over the domain dropped below 10^{-5}.

The other criterion was based on the behavior of two kinds of monitors. One monitor was a point where the temperature was measured. It was located 40 mm from the central axis and 181 mm away from the burner. The second monitor was Area-Weighted Average, which measured the molar fraction of CO_2 on the outlet of the combustor. The desired behavior of monitors was to remain stable in relation to the number of iterations.

RESULTS AND DISCUSSION

The main purpose of this study is to investigate numerically the impact of different burner configurations on the combustion process within the combustor. For this purpose, different configurations were designed. In order to organize the simulation, the different configurations were assigned names as listed in table 3 and test conditions are presented in table 4.

Table 3 Simulated burner configurations.

Configuration	Air inlet diameter D_{air} (mm)	Air fuel inlets distance L (mm)
A (available detailed experimental data)	10	15
B	9	15
C	8	15
D	7	15
E	6	15
F	10	7.5
G	8	7.5
H	6	7.5
I	10	30
J	8	30
K	6	30

Table 4 Test conditions.

Parameter	Value
Input power	10 kW
Excess air coefficient	1.3
Air inlet temperature	673 K
Air inlet velocity	Configurations: A, F, I – 108.47 m/s B – 133.92 m/s C, G, J – 169.49 m/s D – 221.37 m/s E, H, K – 301.31 m/s
Air inlet diameter	Configurations: A, F, I - 10 mm B - 9 mm C, G, J - 8 mm D - 7 mm E, H, K - 6 mm
Air inlet species (mole fraction)	0.21 O_2 0.79 N_2
Air inlet turbulence specification	Turbulent intensity - 5 % Hydraulic diameter = Air inlet diameter

Fuel inlet temperature	298 K
Fuel inlet velocity	6.06 m/s
Fuel inlet diameter	2 mm
Fuel inlet species (mole fraction)	1 CH_4
Fuel inlet turbulence specification	Turbulent intensity - 5 % Hydraulic diameter = Fuel inlet diameter
Outlet pressure	1 atm
Side wall temperature	1421 K
Front wall temperature	1204 K
Inlet ducts wall temperature	1204 K
Wall emissivity (all walls)	0.85

On the foundation of past experimental studies performed on the small-scale combustor (Veríssimo et al. 2011) and on the basis of the fundamental knowledge, the nature of the flow should be explained to gain a better understanding of the presented results. The momentum of the central air jet is large enough to generate a strong reverse flow zone, that recirculates hot flue gas back toward the near-burner region so that the combustion occurs under relatively low oxygen concentrations and relatively low temperatures, which are required to sustain the flameless combustion regime. The central air nozzle momentum is the main driver for the establishment of the desired, flameless combustion regime. The graph of axial temperature and CO profiles are presented in figures 5 and 6.

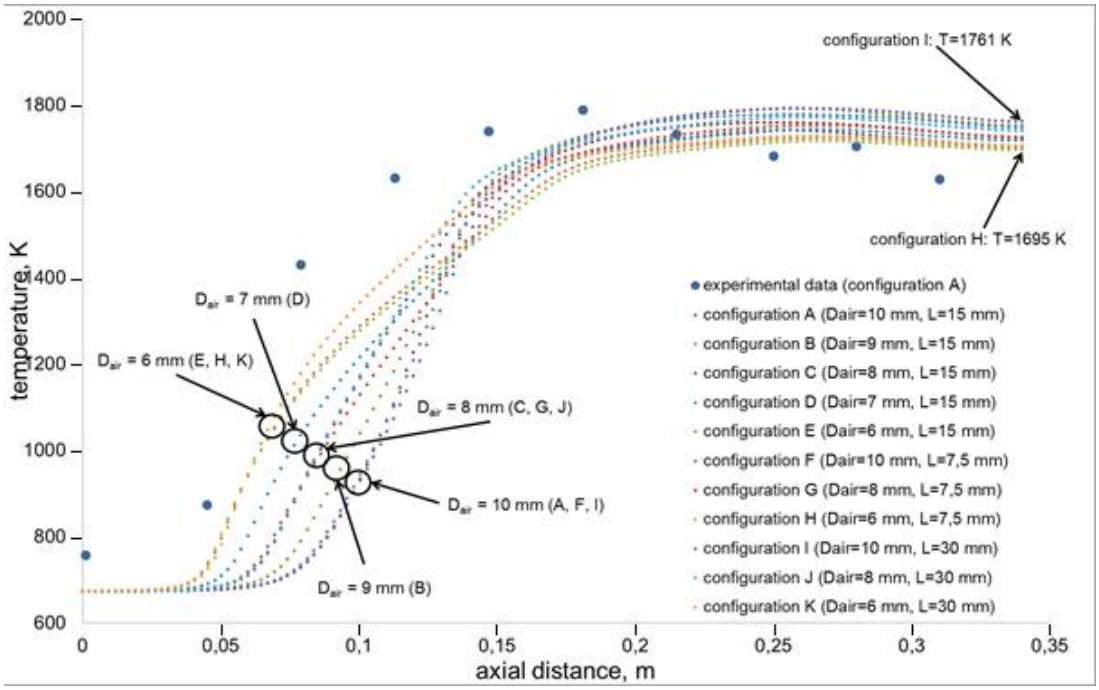

Fig. 4 Predicted and measured axial profiles of mean temperature.

The predictions of axial mean temperature profiles for all the tested configurations reveal, that for burner configurations with smaller inlet air diameter, the decay of the jet occurs quicker and therefore, the main reaction zone and corresponding temperature rise are observed closer to the burner. Despite the relatively large difference in air velocity (301.31 m/s for D_{air} = 6 mm and 108.47 m/s for D_{air} = 10 mm) and different air fuel inlet distance L, the temperature profiles for axial distance over z ≈ 0.15 m are relatively close for all the configurations.

The highest and lowest axial temperatures at the outlet are observed for the most extreme configurations, namely I (D_{air} = 10 mm, L = 30 mm) and H (D_{air} = 6 mm, L = 7.5 mm). The reason for this is that for the configuration I, the main reaction zone is further away from the burner, opposite to the configuration H, where the reaction zone (and the related temperature increase) is closer to the burner. This indicates, that the mixing between fuel and oxidizer is slower for configurations with larger values of L and lower air inlet velocities. The shapes of the profiles at an axial distance from z ≈ 50 mm z ≈ 150 mm reveal, that the initial increase of temperature is mostly dependent on air inlet diameter, because despite different values of air fuel inlet distances L, the profiles with equal values of D_{air} clearly coincide, what is marked in the graph.

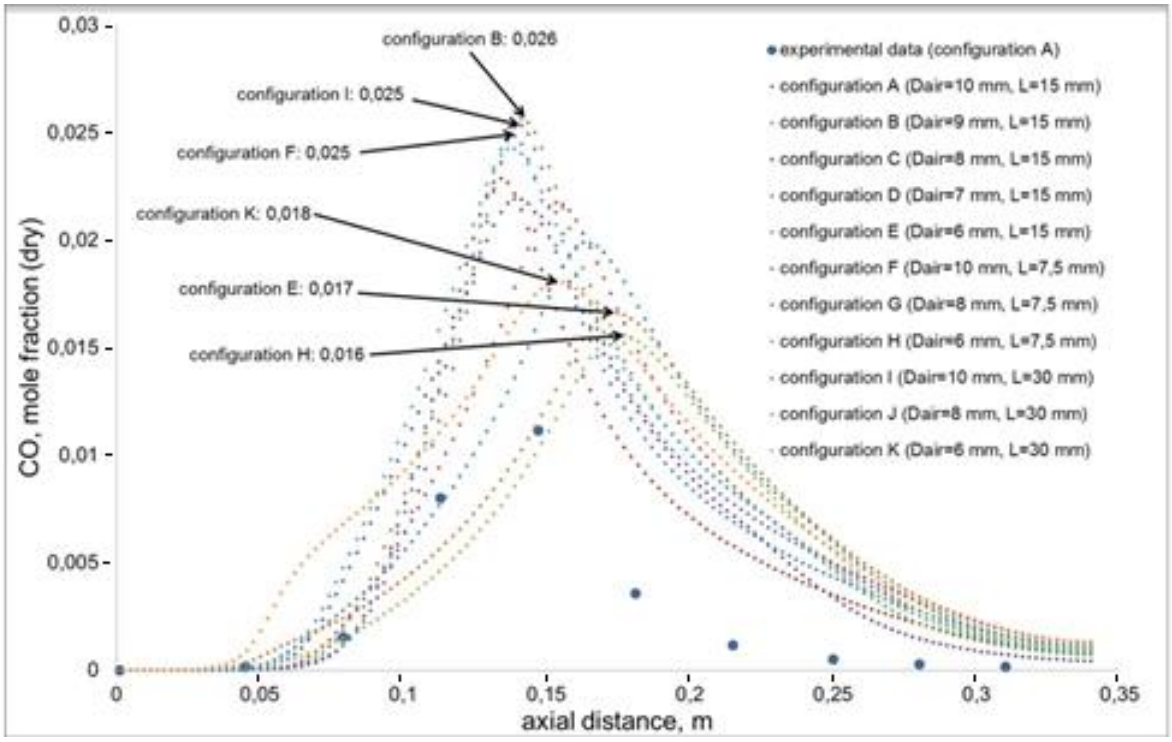

Fig. 5 Predicted and measured axial profiles of CO2, O2, and CO mean molar fractions on a dry basis.

The mean CO molar fraction profiles overestimate the experimental data. Nevertheless, the qualitative prediction is satisfactory, the peak concentration is expected in the similar region, as in experimental measurements. Comparing the predictions for different burner configurations it can be observed, that the lowest peak concentrations are expected for configurations with the smallest air inlet diameter, which can be related to more intense mixing between the oxidizer, fuel and recirculated flue gas for larger air inlet velocities. The lowest peak concentration was predicted for configuration H, where the air and fuel jets are very close to each other, meaning that the fuel stream is quickly sucked by the air stream and reaction takes place faster and with higher oxygen concentration. The highest peak CO concentrations were predicted for configurations with D_{air} equal to 10 and 9 mm (B, F and I).

In figures 6 and 7, the contours of temperature and OH species fields are presented for all tested configurations. High OH concentrations can be correlated with the high intensity of reaction in the given region and therefore it provides a valuable source of information concerning the nature of the combustion process.

More uniform temperature and OH fields are related to the flameless combustion regime, while the presence of regions of very high temperature and OH concentrations signalize the appearance of flame front related to regular combustion regime.

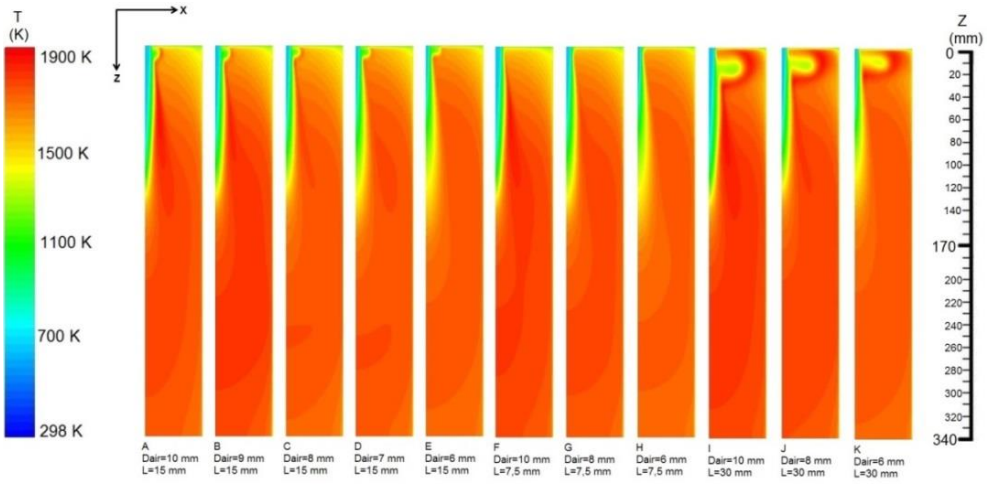

Fig. 6 The contours of predicted temperature fields for all tested configurations.

The temperature fields of configurations A-E reveal that with the decrease of the air inlet diameter, the reaction zone is moved away from the burner and the higher air inlet velocity leads to more uniform temperature field and absence of high temperature regions, which could indicate the presence of flame front. For configurations A-E there is a zone of higher temperature near the burner between z ≈ 0 to 20 mm, and along the inlet air jet between z ≈ 30 mm to 150 mm, which is more stretched and cooler for higher air inlet velocities. The region between z ≈ 0 to 20 mm disappears for configurations F-G, which are the configurations, where the temperature field is the most uniform. When comparing all the configurations it is clear that the combination of the lower air inlet diameter with smaller air fuel inlets distance produces the most uniform temperature field, which can be proven by the temperature field observed in configuration H with the smallest tested air inlet diameter and the smallest distance between the air and the fuel nozzles. The configurations I-K, with a distance of 30 mm yields the least uniform temperature fields with visible high temperature regions possibly indicating the presence of a flame front between z ≈ 0 to 40 mm and along the air jet between z ≈ 30 mm to 150 mm.

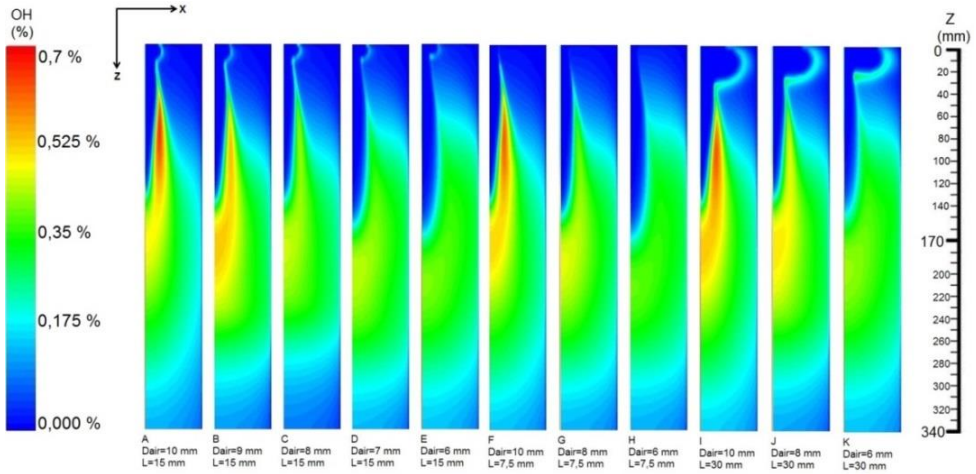

Fig. 7 The contours of predicted OH fields for all tested configurations.

By the OH concentration fields of configurations A-E it can be observed that with increasing air inlet velocity, the combustion process occurs at a larger region and closer to the burner, which indicates, that the intensity of recirculation is correlated with the air jet momentum. The consequence of this is that the reactions are less intense, the region of high OH concentration visible for configuration A is distributed over a larger region for configurations with lower air inlet diameter B-E. This region, marked in different shades of red, is visible for configurations with the air inlet diameter of 10 mm, namely A, F and I. Again, as formerly deducted from the temperature fields, the reaction zone is more uniform for lower air fuel inlet distances, this can be seen for example in the OH fields F-H, where the value of L is equal to 7.5 mm. The best configuration concerning the flameless combustion regime was achieved for configuration H, where both temperature and OH concentrations turned out to be mostly uniform over the whole simulated combustion chamber.

In table 5 the maximum temperatures T_{max}, average temperatures T_{avg} (by volume) and average temperature deviations T* (by volume) are listed. The average temperature deviation is given by:

$$T^* = \frac{|T_{max} - T_{avg}|}{T_{avg}} \quad (1)$$

Table 5 The comparison of maximum, average temperatures and temperature deviations.

Configuration:	T_{max}, K:	T_{avg}, K:	T*:
A	1871	1688	0.109
B	1819	1714	0.061
C	1794	1681	0.067
D	1747	1691	0.033
E	1748	1681	0.040
F	1851	1708	0.084
G	1759	1696	0.037
H	1727	1677	0.030
I	1890	1730	0.093
J	1896	1720	0.103
K	1883	1694	0.111

From the presented data, it can be noticed that, with the exception of configuration B, the lower the air inlet diameter (and therefore higher air jet momentum), the maximum and average temperature decreases, which means that there is stronger recirculation between the flue gas and the reactants producing more leveled temperature field. The same correlation can be found for the fuel inlet nozzle distance L, as the highest peak and average temperatures are noted for the highest distance of L = 30 mm and the lowest for the distance of L = 7.5 mm. The configuration H yields the lowest values of these parameters and also the lowest value of average temperature deviation. These values for configuration H are the most favorable results when it comes to the establishment of the flameless combustion regime, and it can be expected that this configuration would produce the lowest emission of thermal NO_x.

CONCLUSIONS

The numerical simulations of a small-scale combustor operating in the flameless combustion regime were conducted. The main objective of the work was to evaluate the impact of the geometrical changes of the burner, namely the diameter of the air nozzle and the distance between the air and fuel nozzles on the combustion process. All 11 different burner configurations (A-K) were simulated. For configurations A-E, the predictions were compared with experimental data drawn from past studies of Veríssimo et al. (2011 and 2013). In order to evaluate the impact of geometrical changes of air nozzle diameter and fuel nozzle distance on the combustion process. The conclusions are as follows:

- Changing the air inlet diameter at constant excess air coefficient and constant power level induces the change in air inlet velocity. For smaller air inlet diameter (and thus higher air inlet velocity) the decay of the air jet occurs quicker, which is shown by mean temperature and mean velocity axial profiles
- With smaller air inlet diameters the main reaction zone moves closer to the burner region due to more intense entrainment of the gas mixture
- The CO concentrations are overpredicted comparing to experimental data, however, the peak concentrations are in good agreement with the measurements, meaning that the maximum concentration is located in the similar region of the combustor. The lowest peak CO concentrations are observed for configurations with the smallest fuel inlet distance, namely F, G, H with the lowest predicted CO concentration for configuration H (D_{air} = 6 mm, L = 7.5 mm)
- By the temperature contours, OH contours and the information about a maximum temperature, an average temperature, and an average temperature deviation, it is predicted that the most uniform temperature field and lowest maximum temperature is expected for configuration H, which combines the smallest tested air inlet diameter with the lowest tested air fuel inlet distance; the general trend was noticed, that the temperature and OH fields are more uniform by both lower air inlet diameter and lower air fuel inlet distance
- For configurations I-K (D_{air} = 10, 8, 6 mm, L = 30 mm) high temperature and OH regions were predicted, which may mean the presence of flame front, which is not desired in the context of achieving flameless oxidation regime
- The most favorable predictions for the achievement of flameless oxidation regime are for burner configurations with fuel inlet distance of 7.5 mm preferably combined with air inlet diameter of 6 mm as in configuration H

REFERENCES

Cavaliere A., and Joannon M. (2004). Mild Combustion. Progress in Energy and Combustion Science, **30**, pp. 329-366.

https://www.eia.gov/tools/faqs/faq.cfm?id=74&t=11 (access: October 2016)

Kazakov A. and M. Frenklach, http://www.me.berkeley.edu/drm/ (access: October 2016)

Krishnamurthy, N., Paul, P.J., and Blasiak, W. (2009). Studies on low-intensity oxy-fuel burner. Proc. Combust. Inst., **32**, pp. 3139–3146.

Kumar, S., Paul, P.J., and Mukunda, H.S. (2002). Studies on a new high-intensity low-emission burner. Proc. Combust. Inst., **29**, pp. 1131–1137.

Magnussen B. F. (1981). On the Structure of Turbulence and a Generalized Eddy Dissipation Concept for Chemical Reaction in Turbulent Flow, Nineteenth AIAA Meeting, **3**, pp. 269-289.

Menter F. R. (1993). Two-Equation Eddy-Viscosity Turbulence Models for Engineering Applications, AIAA Journal, **32(8)**, pp. 1598-1605.

Mi, J., Li, P., Dally, B.B., and Craig, R.A. (2009). Importance of initial momentum rate and air-fuel premixing on moderate or intense low oxygen dilution (MILD) combustion in a recuperative furnace. Energy Fuels, **23**, pp. 5349–5356.

Pope S. B. (1997). Computationally efficient implementation of combustion chemistry using in situ adaptive tabulation, Combustion Theory and Modelling, **1**, pp. 41-63.

Veríssimo A. S., A. M. Rocha A., and Costa M., M. (2011). Operational, Combustion, and Emission Characteristics of a Small-Scale Combustor, Energy Fuels, **25**, pp. 2469-2480.

Veríssimo A.S., A.M.A. Rocha and M. Costa, M. (2013). Importance of the inlet air velocity on the establishment of flameless combustion in a laboratory combustor, Experimental Thermal and Fluid Science, **44**, pp. 75–81.